Environ Sci Pollut Res (2017) 24:13782–13796
DOI 10.1007/s11356-017-8839-2

RESEARCH ARTICLE

Simultaneous wastewater treatment and bioelectricity production in microbial fuel cells using cross-linked chitosan-graphene oxide mixed-matrix membranes

Shima L. Holder[1] · **Ching-Hwa Lee**[1] · **Srinivasa R. Popuri**[2]

Received: 14 December 2016 / Accepted: 15 March 2017 / Published online: 12 April 2017

Abstract Microbial fuel cells (MFCs) are emerging technology for wastewater treatment by chemical oxygen demand (COD) reduction and simultaneous bioelectricity production. Fabrication of an effective proton exchange membrane (PEM) is a vital component for MFC performance. In this work, green chitosan-based (CS) PEMs were fabricated with graphene oxide (GO) as filler material (CS-GO) and cross-linked with phosphoric acid (CS-GO-P(24)) or sulfuric acid (CS-GO-S(24)) to determine their effect on PEM properties. Interrogation of the physicochemical, thermal, and mechanical properties of the cross-linked CS-GO PEMs demonstrated that ionic cross-linking based on the incorporation of PO_4^{3-} groups in the CS-GO mixed-matrix composites, when compared with sulfuric acid cross-linking commonly used in proton exchange membrane fuel cell (PEMFC) studies, generated additional density of ionic cluster domains, rendered enhanced sorption properties, and augmented the thermal and mechanical stability of the composite structure. Consequently, bioelectricity performance analysis in MFC application showed that CS-GO-P(24) membrane produced 135% higher power density than the CS-GO-S(24) MFC system. Simultaneously, 89.52% COD removal of primary clarifier municipal wastewater was achieved in the MFC operated with the CS-GO-P(24) membrane.

Responsible editor: Bingcai Pan

✉ Srinivasa R. Popuri
popurishrinu@gmail.com

[1] Department of Environmental Engineering, Da-Yeh University, Changhua 51591, Taiwan, People's Republic of China

[2] The University of the West Indies, Cave Hill Campus, Bridgetown 11000, Barbados

Keywords Chitosan · Graphene oxide · Cross-linking · Microbial fuel cell · Proton exchange membrane · Wastewater treatment

Introduction

Dual-chambered microbial fuel cells (MFCs) work by utilizing electrochemically active microorganisms to break down organic matter present in the anode chamber through a series of metabolic pathways. During this oxidation of organic matter, electrons and protons are produced and transported to the cathode chamber; the electrons, via an electrical circuit, are accepted by electron acceptors present in the catholyte; meanwhile, protons diffuse toward the cathode chamber through a proton exchange membrane (PEM) (Jiang et al. 2011). Due to the oxidation and reduction reactions occurring at the anode and cathode chambers, respectively, a potential difference exists, allowing electrical current to flow through the external circuit, thereby producing power (Peighambardoust et al. 2010; Logan et al. 2006). Simultaneous wastewater treatment and energy production is the attractive function of non-fossil-fuel-based MFC technology, especially considering that 100,000 L of wastewater per day could theoretically generate 24,758 kWh of energy (Fornero et al. 2010).

In MFC research, many efforts have been directed to the selection of viable membrane materials for effective and rapid transportation of protons from the anode to cathode chamber, while ensuring separation between the two chambers that prevents oxygen and substrate crossover and avoids electrical short circuiting (Oh et al. 2004; Velasquez-Orta et al. 2011; Zhu et al. 2011). The PEM is therefore a vital component, and its function, a crucial factor in MFC technology for ensuring satisfactory bioelectricity performance and stability (Liu and Logan 2004; Min et al. 2005).

Commercial PEMs have been used in fuel cell technological applications to increase efficiency due to the high proton conductivity through such membranes (Sen et al. 2013; Shahgaldi et al. 2014; Smitha et al. 2005; Ilbeygi et al. 2015), in recent years. Nafion, a popular perfluorinated sulfonated polymer, has been perceived as the most suitable proton conductive membrane due to the high proton conductivity of the membrane in fully hydrated states, excellent chemical stability, and mechanical strength (Peighambardoust et al. 2010). However, Nafion is expensive, exhibits decreased proton conductivity at temperatures above 80 °C, high crossover of methanol, high electro-osmotic drag, and has other drawbacks (Ahn et al. 2017; Dupuis 2011; Liu et al. 2016). Recent research has shown that increased content of fixed ions in sulfonated polymers with a high degree of sulfonation renders increased proton releasing abilities due to the supplementation of proton carrier concentration in an acidic water medium (Xie et al. 2015). High sulfonation, however, also results in excessive water swelling, thereby allowing oxygen and substrate crossover (Bakangura et al. 2016). Accordingly, cross-linking has been used as a good solution to maintain a proper sulfonation level or water uptake content and simultaneously to enhance mechanical properties (Higa et al. 2015; Liang et al. 2015; Zhao et al. 2016). This indicates that the effect of water uptake in PEMs should be considered heavily as the proton conductivity and cation exchange capacity of membranes depend upon sorption properties (Kim et al. 2006; Peighambardoust et al. 2010; Sasikala et al. 2016; Rudra et al. 2015). These studies provide evidence that physical and chemical cross-linking are equally as important in PEM synthesis toward improved MFC bioelectricity performance.

Hydrophilic polymers, in the context of eco-friendliness and water sorption abilities, have been recognized and selected as alternative membrane material for the PEMs used in MFC technology (Shaari and Kamarudin 2015). Chitosan (CS) membranes, in particular, are one type of cationic polysaccharide membranes widely used in membrane separation technology; however, the hydrophilicity of CS leads to significant membrane swelling in aqueous solution and a subsequent decline in selectivity and mechanical strength (Ma and Sahai 2013; Shaari and Kamarudin 2015). To overcome these drawbacks, several researchers have modified chitosan membranes via grafting (Jayakumar et al. 2005), blending (Hajji et al. 2016; Xiong et al. 2008), and cross-linking (Beppu et al. 2007) for use in pervaporation studies (Rao et al. 2007), desalination (Padaki et al. 2012), and fuel cell (Holder et al. 2016) applications.

Considering low costs, eco-friendliness, non-toxicity, abundance, and chemical stability (Ma and Sahai 2013), CS is therefore a pleasing alternative to the more expensive synthetic PEMs. Furthermore, owing to the presence of amino groups amenable to undergoing chemical modifications, CS is easily modifiable and as a PEM does not require the conditioning treatment necessary for the popular Nafion-based membranes. Recently, CS has also been prepared as mixed-matrix membranes by combining with inorganic materials such as carbon nanotubes (Bai et al. 2014; Thakur and Voicu 2016; Venkatesan and Dharmalingam 2013) and graphene oxide (GO) (Azarniya et al. 2016; Pan et al. 2011; Shirdast et al. 2016) to improve its properties toward improved physicomechanical functionality (Bakangura et al. 2016). Among these, GO addition to the CS matrix is widely used as the emerging filler, and interestingly, the majority of the modified membrane materials are cross-linked with sulfuric acid.

To the authors' best knowledge, most studies employ the use of sulfuric acid as the main cross-linker to various synthetic polymer membranes in MFC application. The current research therefore aimed to compare the use of phosphoric acid and sulfuric acid as cross-linkers for CS and CS-GO, finding the more suitable cross-linking agent that renders enhanced physicochemical, mechanical, and thermal properties. Albeit cross-linking is a well-known approach, there are still not many studies exploiting broadly the role of cross-linking agents in the emerging CS-GO mixed-matrix membranes. The influence of cross-linking agent on membrane properties was thoroughly evaluated through characterization studies such as Fourier transform infrared (FTIR)-attenuated total reflectance (ATR) spectroscopy, X-ray diffraction (XRD), thermogravimetric analysis (TGA), cation exchange capacity (CEC), tensile strength and elongation, and sorption analyses. Additionally, the performance of the cross-linked CS-GO membranes was evaluated in MFC studies for simultaneous bioelectricity production and chemical oxygen demand (COD) removal for wastewater treatment.

Materials and methods

Materials

Analytical grade glacial acetic acid, isopropyl alcohol, orthophosphoric acid, L-cysteine, and potassium ferricyanide were purchased from Katayama Chemical Co. Ltd. (Taiwan). CS was obtained from Marine Bio Resources Co. Ltd. (Thailand) and used as a membrane matrix material. The molecular weight (approx. 200 kDa) and Brookfield viscosity (59 cps at 1 wt% in 1% acetic acid) of the CS were reported by the supplier. The degree of deacetylation (DDA) of the CS was determined as 67.04 ± 0.06% using FTIR-ATR analysis (Holder et al. 2016). Natural graphite powder was purchased from Sigma-Aldrich Co. Ltd. All other materials and solvents (Sigma-Aldrich) were used without further purification. Deionized water was used throughout the study.

Synthesis of GO nanosheets

GO nanosheets were indigenously synthesized using the modified Hummers method (Hummers and Offeman 1958).

Graphite powder (2 g) was mixed with 1 g sodium nitrate ($NaNO_3$) and 46 mL concentrated sulfuric acid (H_2SO_4) in a 250-mL round-bottom flask under magnetic stirring for 20 min at 5 °C. Slowly, 6 g potassium permanganate ($KMnO_4$) oxidizing agent was added while stirring vigorously for 15 min. The mixture was then heated at 35 °C for 1 h. Deionized water (92 mL) was added dropwise to generate a significant amount of heat and gas rapidly, and the mixture was maintained at 95 °C for 1.5 h. Finally, deionized water (280 mL, 60 °C) was added along with 3 wt% hydrogen peroxide (H_2O_2). As the addition of H_2O_2 facilitates removal of remaining traces of $KMnO_4$, the H_2O_2 was added dropwise until the absence of bubbles and a yellow color occurred, verifying the neutralization of $KMnO_4$. The solution underwent ultrasonication for 30 min. Centrifugation of the mixture was carried out (6000 rpm, 45 min), and the liquid portion was discarded. The resultant product was neutralized to pH 7 with deionized water followed by freeze-drying to obtain GO in the form of a dark brown powder. The resulting GO powder was dispersed in 100 mL deionized water to form 5 wt% GO solution followed by exfoliating the GO particles into GO nanosheets via ultrasonication.

Fabrication of CS-GO mixed-matrix composite membranes

Chitosan solution was prepared by dissolving 2 g of CS in 2 wt% acetic acid solution at 80 °C. A casting solution containing CS and the above-prepared GO (5 wt%) nanosheets (1:1) was prepared by stirring under constant temperature at 60 °C for 4 h until a thick viscous liquid was formed. The resultant homogenous bubble-free CS-GO mixture was casted onto a clean glass plate and allowed to dry in a vacuum oven at 45 °C overnight. The fabricated membrane was removed carefully and stored in a desiccator.

Phosphorylation or sulfurization of CS-GO mixed-matrix composite membranes

Cross-linking of CS-GO membranes was carried out with 25 mL of 85 wt% phosphoric acid in an isopropanol-water bath (Holder et al. 2016) for 24 h and labeled CS-GO-P(24). Similarly, 5.53 mL of 96.4 wt% sulfuric acid was used as another cross-linking agent for CS-GO membranes, and the resulting membrane was labeled CS-GO-S(24). It should be noted that pristine CS membranes cross-linked via the aforementioned procedure were prepared in order to elucidate the exact role of phosphorylation and sulfurization on the properties and characteristics of CS. The resulting membranes were labeled as CS, CS-P(2), CS-P(24), CS-S(2), and CS-S(24) according to cross-linking time.

Membrane characterization

The physicochemical properties of the prepared membranes were characterized by FTIR-ATR spectra. The DDA of the CS powder used throughout this study was determined using the absorbances at 1320 and 1420 cm^{-1} (A_{1320} and A_{1420}, respectively) of the FTIR-ATR spectra and calculated using the following equation (Brugnerotto et al. 2001; Czechowska-Biskup et al. 2012):

$$\mathrm{DDA}\ (\%) = 100 - [(A_{1320}/A_{1420}) - 0.03822]/0.03133 \quad (1)$$

The membranes were investigated using an X-ray diffractometer (Shimadzu XRD-6000). X-rays of wavelength 1.540 Å were generated by a Cu Kα source. The angle of diffraction was varied in the range of 5°–60° at the rate of 2° min^{-1}.

The morphologies of all fabricated membranes were characterized using a multi-function field emission scanning electron microscope (SEM, Joel JSM-6400) and energy-dispersive X-ray spectroscopy (EDS, PentaFETx3-7585 EDS).

Thermal stability curves of the membranes were determined using a self-designed thermodestructive analyzer at Da-Yeh University. The sample with a weight of 0.05 g was heated from 27 to 550 °C at a heating rate of 10 °C/min in nitrogen atmosphere.

Mechanical testing

Mechanical properties were investigated using tensile testing to determine the strength of the fabricated membranes. The tensile strength and elongation at break of each membrane were measured using a Shimadzu E2 Test (model E2-LX) tensile strength tester with a load cell of 2 kN at the rate of 12.5 mm/min. Using a film cutter, the membranes with known width (10 mm) and thickness were shaped according to the requirements of the instrument. Each membrane was clamped between the grips of the tensile tester with 50-mm gap length. The tensile strength (σ) and elongation (ε) were calculated according to Eqs. (2) and (3):

$$\sigma = L/A \quad (2)$$

$$\varepsilon = \left(L_f/L_i\right) \times 100 \quad (3)$$

where L and A are the applied load and membrane cross-sectional area, respectively, and L_f and L_i are the membrane lengths after and before tensile strength testing, respectively.

Sorption studies

Sorption (S) of the membranes with MFC feed wastewater was determined using a conventional gravimetric method. The membranes (2 × 2 cm^2) were cut and placed in an oven at 25 °C for 12 h. The dried membranes were weighed (W_d)

and immersed in a 50-mL beaker of MFC feed wastewater at room temperature. After 24 h, the samples were removed from solution, wiped to remove excess liquid from the surface, and quickly weighed (W_W). Final uptake values using the average of three measurements were determined using Eq. (4). The area swelling (AS) was measured in the plane direction and calculated by Eq. (5):

$$S = [(W_W - W_d)/W_d] \times 100 \quad (4)$$

$$\mathrm{AS} = [(A_W - A_d)/A_d] \times 100 \quad (5)$$

where W_W and W_d are the weights of the wet and dry membranes, respectively, and A_W and A_d are the areas of the wet and dried membranes, respectively.

Cation exchange capacity

Cation exchange capacities (CECs) of the membranes were investigated in order to determine the effect of cross-linking on the CS and CS-GO PEMs. CEC indicates the number of groups present before and after cross-linking, thereby suggesting the extent of cross-linking by giving the number of milliequivalents of ions per gram of dry membrane. Membranes of identical size (2×2 cm^2) in acid (H^+) form were converted to sodium ion (Na^+) form by immersing in NaCl (1 M, 50 mL) solutions for 24 h at room temperature to liberate H^+ ions. The protons in solution were then titrated against 0.1 M NaOH, and phenolphthalein was used as the pH indicator. CEC in milliequivalents per gram was calculated by Eq. (6) (Fu et al. 2015).

$$\mathrm{CEC} = (M_{\mathrm{NaOH}} \times \mathrm{V}_{\mathrm{NaOH}})/W \quad (6)$$

where M_{NaOH} is the molarity of NaOH solution, V_{NaOH} is the consumed volume of NaOH solution, and W is the membrane sample weight.

Oxygen mass transfer assay

The oxygen mass transfer coefficients for the fabricated mixed-matrix membranes were studied using a portable dissolved oxygen (DO) probe (WA-2017SD, Lutron Electronic Enterprise Co. Ltd., Taiwan). For the determination of oxygen mass transfer coefficient, an un-inoculated two-chambered bottle MFC reactor fitted with the desired membrane and filled with distilled water was used. The cathode chamber was continuously aerated to maintain saturated DO condition, while anaerobic conditions were maintained in the anode chamber. The mass transfer coefficient of oxygen in the membrane (K_o) was determined by monitoring the DO concentration over time using Eq. (7) (Kim et al. 2007):

$$K_o = -(V/A \times t) \times \ln\left[\left(C_{1,0} - C_2\right)/C_{1,0}\right] \quad (7)$$

where V is the volume of solution in the MFC, A is the membrane cross-sectional area, $C_{1,0}$ is the saturated concentration in water and C_2 is the measured DO in the MFC at time, t.

The oxygen diffusion coefficient (D_o) for each membrane was subsequently calculated as:

$$D_o = K_o \times L_t \quad (8)$$

where L_t is the membrane thickness.

Bioelectricity production

MFC construction and operation

Dual-chambered MFCs were fabricated using media bottle (450 mL working volume, Jin-Lan Equipment Company, Taiwan) with 4.52-cm^2 effective membrane area, and both chambers outfitted with carbon rods (projected surface area 0.019 m^2) connected to copper wire. Municipal wastewater collected from the primary clarifier of a local municipal wastewater treatment plant was used for anodic chamber inoculation and acclimatization. All MFCs were operated with fed-batch cycles at 30 ± 1 °C.

Cell voltages were recorded using Lutron 3 Channel Voltage Recorder (MMV-387SD, Lutron Electronic Enterprise Co. Ltd., Taiwan) across an external resistance (R, 1000 Ω). At the defined cycle end, the resistance was varied stepwise to determine power generation as a function of load. Current (I) was calculated using Ohm's law:

$$I = V/R \quad (9)$$

where V is the voltage and R is the external resistance.

Power (P) was calculated using the following equation:

$$P = I \times V \quad (10)$$

As previously described (Holder et al. 2016), one fed-batch cycle was defined as the time from MFC influent introduction to two successive days of voltage decline. The internal resistance (R_{int}) and power density curve (normalized according to the reactor volume based on the fuel cell dimensions expressed in mW/m^3) of each MFC were determined using the polarization curve method (Logan et al. 2006) by varying the external resistance and recording the respective voltage and current outputs. The pH and conductivity of the MFC influent and effluent were recorded using a multi-functional Lutron pH/ORP, CD/TDS, salt meter (WA-2017SD, Lutron Electronic Enterprise Co. Ltd., Taiwan). COD was measured using standard methods (APHA 2005).

Results and discussion

Membrane characterization

Fourier transform infrared spectroscopy

FTIR was used to characterize the changes in membrane functional groups before and after modification. The FTIR spectra of plain and cross-linked CS membranes are presented in Fig. 1a, and the cross-linked CS-GO membranes in Fig. 1b. Characteristic absorbance bands of chitosan can be seen in Fig. 1a where a broad band associated with –OH was visible around 3286 cm^{-1}, along with prominent peaks associated with C–H groups at 2856 cm^{-1} and N–H groups at 1452 cm^{-1} (Cadogan et al. 2015; Liu et al. 2005; Ordikhani et al. 2015; Rao et al. 2007). These characteristic peaks were reflected in the cross-linked membranes; however, cross-linking with acid groups was confirmed by the broadening of the –OH band and lower wavenumber shift of the amide band in all membranes, regardless of acid group present (phosphoric acid or sulfuric acid). Upon cross-linking reaction between the strong nucleophilic amino groups of chitosan and the phosphate groups of phosphoric acid, the chitosan chains formed an antiparallel structure. This cross-linking reaction is responsible for the strong ionic bonding that occurs between the NH_3^+ functional groups of the chitosan and the PO_4^{3-} or SO_4^{2-} acid group of the cross-linking solution (Rao et al. 2007).

GO was successfully synthesized from the oxidation of graphite as shown in Fig. 1b, and all functionalized groups generated on the GO surface due to the oxidation process were confirmed. The presence of oxide functional groups in GO was confirmed by a peak at 1148 cm^{-1} which is attributed to –C–O of –C–OH band, while the stretching vibrations of –C–O of C–O–C were visible at 1028 cm^{-1}. The –C=C– band showing the sp^2 character present in pure graphite remained after oxidation, and peaks were observed in the 1615–

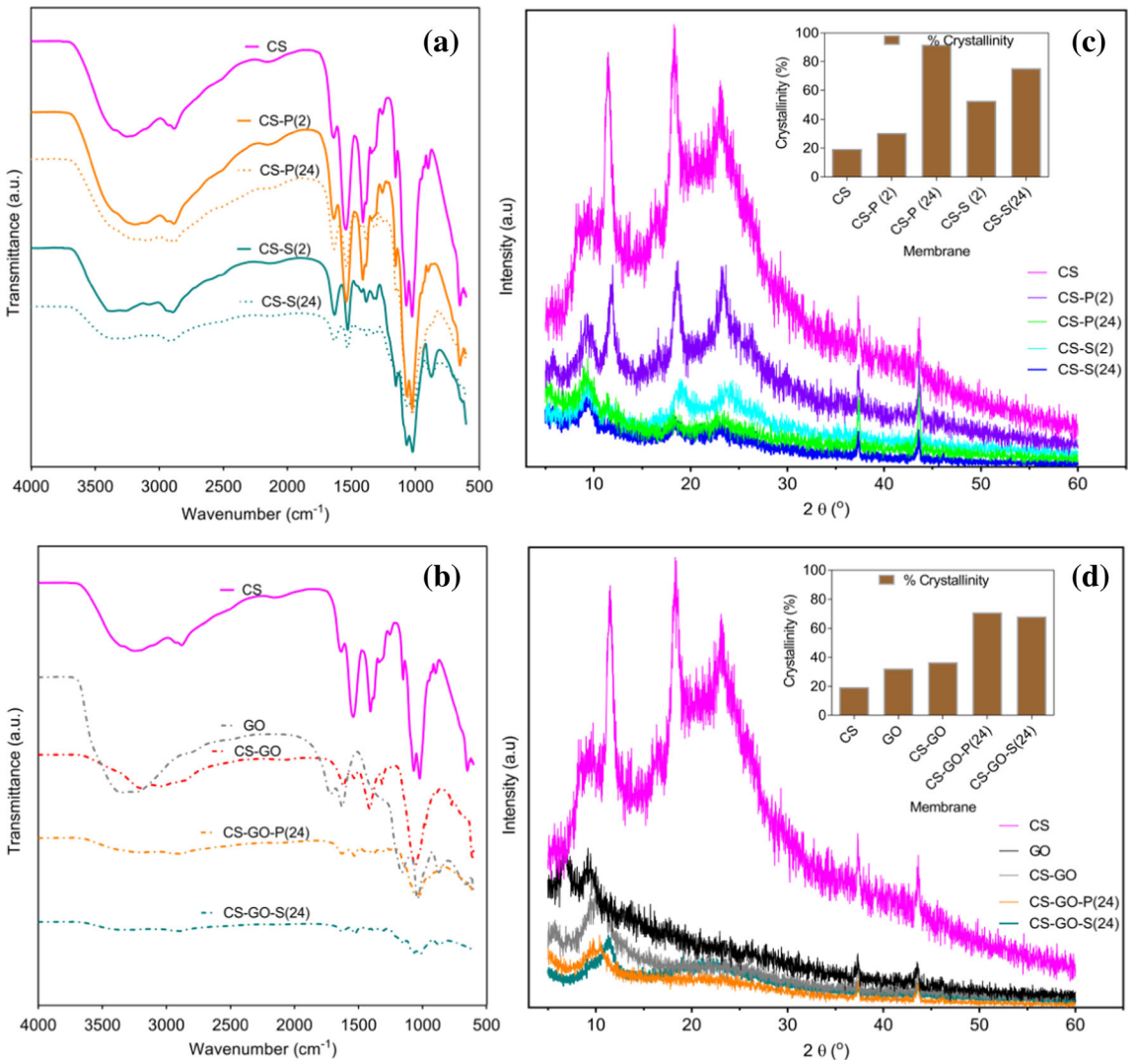

Fig. 1 FTIR-ATR spectra (**a**, **b**) and XRD patterns with the respective crystalline percentages (**c**, **d**) of pristine CS and CS-GO cross-linked membranes, respectively

1677 cm^{-1} range of GO (Krishnamoorthy et al. 2012; Paulchamy et al. 2015). The broad peak at 2822–3678 cm^{-1} attributed to the O–H stretch of water molecules indicated that water was absorbed by GO (Paulchamy et al. 2015).

The addition of GO to CS resulted in the characteristic GO adsorption peak that shifted to a lower number (3169 cm^{-1}) and broadened, confirming the interaction of GO with chitosan; a combination of characteristics of the CS and GO peaks was observed. Cross-linked CS-GO composites (CS-GO-P(24) and CS-GO-S(24)) both exhibited a shift of the amide band to lower wavenumbers, as well as P=O and S=O stretching that resulted in –OH deformation around 1373 and 1393 cm^{-1}, respectively, confirming acid group ionic chain cross-linking with the chitosan chains (Shanmugam et al. 2016). Broadening of the –OH peak was denoted for both cross-linked CS-GO membranes, indicating a strong interaction with the –OH groups of CS to the –OH groups of phosphoric or sulfuric acid and water. FTIR investigation therefore affirmed the presence of linkage between chitosan and GO through intermolecular hydrogen bond formation and confirmed cross-linking of CS-GO with phosphoric or sulfuric acid groups.

The DDA of CS used throughout this study was determined as 67.04 ± 0.06%. This value should be considered in the future or comparative CS membrane studies, as low DDA results in a less compact chitosan structure that affects ionic bonding and, by extension, physicochemical and mechanical properties; the opposite is true for high DDA (de Moura et al. 2011; Feng et al. 2012).

X-ray diffraction analysis

XRD patterns and crystallinities of the cross-linked CS and CS-GO films are illustrated in Fig. 1c–d. It could be noted that the characteristic structure of CS was confirmed with strong diffractions around $2\theta = 9°$ and 11.42° and the broad amorphous peak around $2\theta = 20°$ (Rao et al. 2007; Liu et al. 2013). Peaks attributed to –OH and $–NH_2$ functional groups were observed around 11.4° and 20° upon cross-linking CS with phosphoric acid and sulfuric acid groups. While the semi-crystalline nature of the plain CS membrane was maintained regardless of cross-linking agent and time, the crystallinities of the CS membranes increased upon cross-linking and even more with increased cross-linking time; the CS-P(24) membrane exhibited higher crystallinity than CS-S(24) membrane.

Successful conversion of graphite to GO shown as a strong peak of GO appeared at $2\theta = 7.5°$ (Fig. 1d) compared to the peak of pristine graphite that appears at $2\theta = 26°$, as reported in the literature (de Moraes et al. 2015; Ordikhani et al. 2015; Yadav and Ahmad 2015). After loading GO into the CS matrix, peaks at the same angles of diffraction characteristic of CS remained; this suggests strong interactions between GO and CS. Subsequent to the cross-linking of CS-GO membranes, similar peaks occurred around $2\theta = 11.26°$ and 22.3° for CS-GO-P(24) and $2\theta = 11.94°$ and 21.7° for CS-GO-S(24), respectively; these peaks are all characteristic of CS.

The incorporation of GO into the CS matrix resulted in a slight increase in crystallinity (from 19.43% in CS to 36.53% in CS-GO), and the phosphorylated CS-GO membrane exhibited higher crystallinity (70.82%) than the sulfurized CS-GO membrane (67.96%). This result suggests that the amorphous portion of the CS-GO structure was more compact due to the decrease in intermolecular distance after phosphorylation. The lower crystallinity observed in CS-GO-S(24) may be attributed to strong interactions of the –OH groups of CS and water, GO and water, and CS and GO being tremendously weakened by the strong ionic bonds which occurred upon cross-linking with the strong acid (sulfuric acid); this effect is commonly observed in plasticized membranes (Holder et al. 2016; Liu et al. 2013). As increased degree of crystallinity effects an increase in membrane physical properties (de Moura et al. 2011), the phosphorylated pristine-CS and CS-GO membranes are anticipated to exhibit the highest tensile strengths.

Surface morphology

Developed interactions between chitosan and GO and the effect of cross-linking on the membrane material were examined by SEM and shown in Fig. 2. It was observed that the morphology of the cross-linked CS sheets (Fig. 2b–e) was smooth, indicating excellent interaction of chitosan with both cross-linking agents. Despite the rough surface appearing with the cross-linked CS-GO mixed-matrix composite membranes, the surface morphologies appear relatively homogenous, suggesting their miscibility and compatibility with each other.

EDS analysis confirmed the presence of phosphorus in CS-GO-P(24) (Fig. 2g) and sulfur in CS-GO-S(24) (Fig. 2h) membrane structures, thereby confirming successful cross-linking action. For both membranes, the degrees of substitution (DS) shown in Table 1 were determined based on the ratio of phosphorus or sulfur to nitrogen content in order to normalize for the substitution of acid groups onto the chitosan amine functional groups (Tachaboonyakiat et al. 2010). This normalization facilitates comparison of the degree of acid group substitution to the chitosan structure in CS-GO-P(24) and CS-GO-P(24) membranes. The physicochemical, thermal, and mechanical properties of the fabricated CS-GO composites are subjected to DS of 5.90 ± 3.69 and 1.54 ± 1.15 for CS-GO-P(24) and CS-GO-S(24) PEMs, respectively. Notably, the DS in the CS-GO-S(24) membrane was lower than that in the CS-GO-P(24) membrane. This corroborates the trends in crystallinities discussed for the same membranes.

Thermogravimetric analysis

Thermogravimetric analysis is an excellent method for the determination of thermal degradation of composite sheets. Figure 3

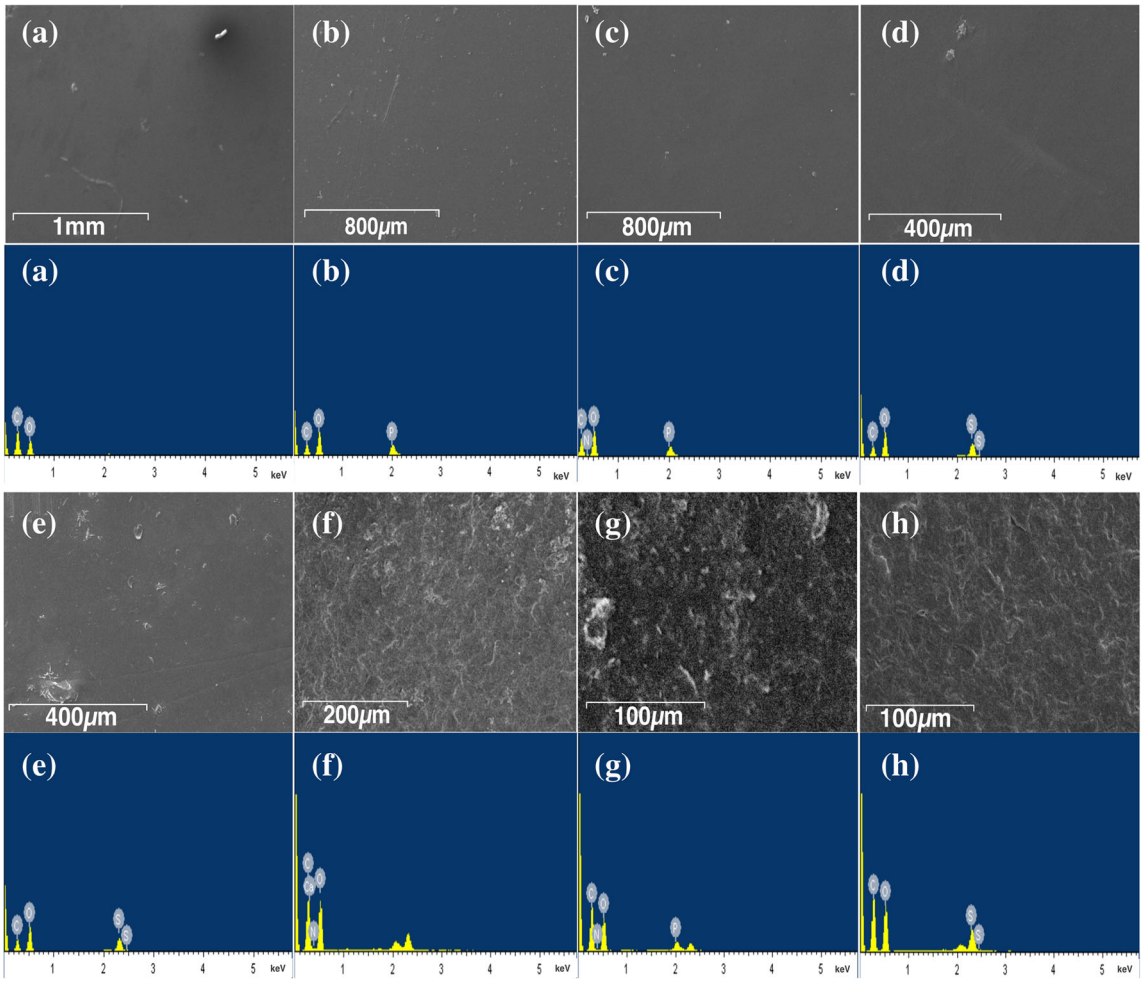

Fig. 2 SEM images and EDS spectra for CS (**a**), CS-P(2) (**b**), CS-P(24) (**c**), CS-S(2) (**d**), CS-S(24) (**e**), CS-GO (**f**), CS-GO-P(24) (**g**), and CS-GO-S(24) (**h**) membranes

shows the thermal degradation temperatures for all synthesized membranes, and the weight loss percentages of the samples are provided in Table 2. Results of the cross-linked CS membranes indicated that both phosphoric acid CS membranes (CS-P(2) and CS-P(24)) exhibited higher thermal stability, shown by increased degradation temperatures, than the sulfuric acid CS membranes (CS-S(2) and CS-S(24)). The effect of cross-linking time on CS membranes showed a particularly strong impact on thermal stability of phosphorylated membranes such that the thermal stability notably enhanced with time.

Table 1 Effect of cross-linking agent and reaction time on the degree of substitution in pristine CS and CS-GO membranes

Membrane	Degree of substitution
CS-P(2)	1.88 ± 0.22
CS-P(24)	6.59 ± 5.87
CS-S(2)	2.08 ± 0.28
CS-S(24)	1.78 ± 0.48
CS-GO-P(24)	5.90 ± 3.69
CS-GO-S(24)	1.54 ± 1.15

Pure GO lost 42% of its weight during in the first decomposition stage from 110 to 170 °C, characterizing free water elimination (Justin and Chen 2014). Initial weight loss in the

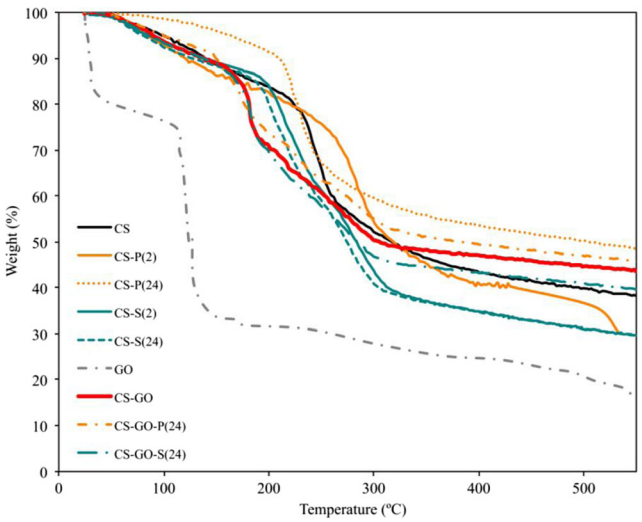

Fig. 3 TGA thermograms of the synthesized membranes

Table 2 Thermogravimetric data and percent weight loss of the fabricated membrane samples

Membrane	$T_{10\%}$ (°C)	$T_{30\%}$ (°C)	$T_{50\%}$ (°C)	$T_{60\%}$ (°C)
CS	138	242	318	467
CS-P(2)	119	269	318	431
CS-P(24)	206	241	503	811
CS-S(2)	137	228	281	310
CS-S(24)	124	219	272	301
GO	29	67	124	129
CS-GO	138	205	304	711
CS-GO-P(24)	149	220	383	785
CS-GO-S(24)	137	195	283	496

CS-GO membrane was attributed to the decomposition of oxygenated functionalities present on GO layer (143–204 °C). The region between 129 and 330 °C could be ascribed to the characteristic thermal degradation of CS as well as the remaining functional groups of GO. GO decomposed at approximately 170 °C, whereas the decomposition of CS-GO in the blended film occurred at a higher temperature (304 °C), indicating the strong linkage between GO and chitosan confirmed by FTIR analysis. Cross-linking the CS-GO membrane with phosphoric acid groups resulted in a membrane that exhibited degradation from 48 °C onward, with major weight loss occurring from 227 °C due to oxidation with increasing temperature and time. In both CS-GO-P(24) and CS-GO-S(24), all oxygen-containing groups were decomposed over 340 °C, and no large changes in weight loss were recorded with an increase in time. By 544 °C, 55% of CS-GO-P(24) had undergone thermal degradation, while at the same temperature, 61% of CS-GO-S(24) had degraded. This suggests that the incorporation of PO_4^{3-} into the CS-GO structure rendered better thermal stability than the incorporation of SO_4^{2-}. CS-GO-P(24) is therefore a good potential candidate as an anhydrous PEM in MFCs operated at high temperatures; these properties are due to the high water-binding energy (47.3 kJ/mol) of phosphoric acid as stated in the literature (Bai et al. 2015; Paddison et al. 2006).

Mechanical testing

Mechanical behavior of the membranes at room temperature was observed using tensile testing and presented in Fig. 4. Coulombic interactions, which occur through cross-linking with acid groups, promoted the formation of strong ionic bonds in the membrane. These bonds caused the polymer chain and acid groups to be entangled, thereby reducing polymer chain mobility after cross-linking, regardless of cross-linking agent used. More specifically, the rigid interlocking structure of the ionically bonded amide and phosphate groups allowed both phosphorylated CS and CS-GO membranes to exhibit higher tensile strengths and lower elongation values

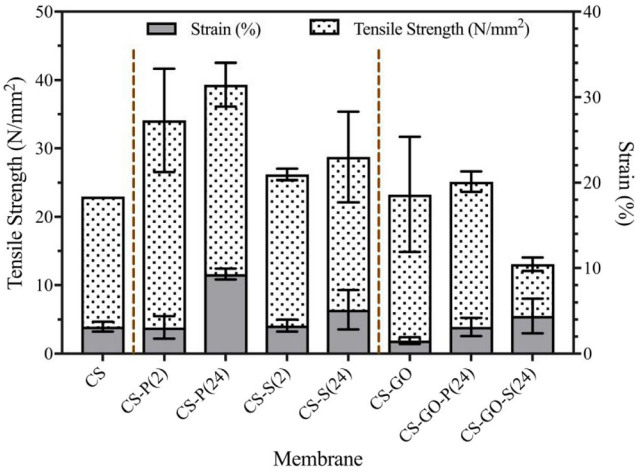

Fig. 4 Tensile properties of the pristine CS and CS-GO cross-linked membranes

than the sulfurized CS and CS-GO membranes. Figure 4 also shows the increasing trend of cross-linking time such that the membranes cross-linked for 24 h exhibited higher tensile strengths than those cross-linked for 2 h; the effect of intermolecular forces led to the rise in tensile strength. Accordingly, CS-P(24) membrane exhibited the highest stress resistance of the cross-linked CS membranes, while CS-S(2) membranes exhibited the least value.

The interfacial interactions and hydrogen bonding which occur upon addition of GO to CS promote an enhancement of the tensile properties of the chitosan matrix; as hypothesized based on XRD analysis, an overall increment in mechanical properties was observed (Mazaheri et al. 2014). In coherence with results observed with the cross-linked CS membranes, the phosphorylated CS-GO composites exhibited more favorable mechanical strength (25.13 ± 1.47 N/mm^2 tensile strength and 3.92 ± 1.32% elongation) for withstanding the hydrostatic pressure of MFC influent than the sulfurized CS-GO composites, which exhibited tensile strength and elongation values of 13.07 ± 0.99 N/mm^2 and 5.53 ± 2.52%, respectively. This is evidence that phosphoric acid cross-linking groups caused increased membrane rigidity, compactness, and mechanical strength of the membranes for MFC studies, compared to the more commonly used sulfuric groups. Furthermore, the results of elongation and tensile strength of sulfurized CS-GO membranes suggest that cross-linking with sulfuric acid incurs some flexibility of the CS-GO structure as described in the XRD analysis.

It should be noted that the GO content was used as 5% throughout this study. While the percentage of the GO influences the tensile strength and thermogravimetric degradation trends of the resulting CS-GO membranes (Han et al. 2011; Mazaheri et al. 2014; Yang et al. 2010), the results for CS-GO, CS-GO-P(24), and CS-GO-S(24) are still comparable with each other for this data set. In comparing the phosphorylated CS membranes with phosphorylated CS-GO membranes, and the same for the sulfurized CS and CS-GO membranes, the

lower tensile strengths observed with cross-linked CS-GO membranes than cross-linked CS membranes can therefore be largely attributed to the high GO% addition in the CS structure; this can be remedied in future works by hybridizing with a more optimal percentage of GO.

Overall, results exhibited that longer cross-linking time (24 h) generally improved the mechanical properties of the CS membrane. Particularly, the use specifically of PO_4^{3-} groups to cross link the CS and CS-GO membranes for 24 h provoked the greatest enhancement of mechanical properties.

Sorption studies

Sorption trends give an idea of the MFC feed solution uptake ability of the synthesized membranes. As the wastewater molecules provide the proton medium (free water), form proton-hopping hydrogen-bonded networks (bound water), and dissociate conducting groups (free water), the uptake of water in PEM therefore facilitates the proton transport process. A PEM should be able to restrict oxygen and substrate transfer but, most of all, allow sufficient sorption to facilitate proton transport while avoiding over-swelling which decreases proton selectivity due to sorption coupling. As the Grotthuss transport/proton hopping and diffusion mechanisms in the hydrated state are highly accepted as the proton transport pathways from anode to cathode (Liu et al. 2016; Chen et al. 2016), performance of the PEMs in MFC operation is highly correlated to their sorption behavior.

Sorption trends of the cross-linked CS and CS-GO membranes are shown in Fig. 5a. Due to its highly hydrophilic nature, the amount of equilibrium sorption was highest in plain CS membranes (97.4 ± 0.7%) compared with the other synthesized PEMs under the same conditions. The incorporation of negatively charged fixed ions (phosphoric acid or sulfuric acid) into the CS membrane structure not only enhanced physicomechanical properties, but the more compact structure of the membranes also effected a reduction in accommodation for feed solution; consequently, sorption was reduced to more acceptable values. As cross-linking time increased, sorption in the membrane was further reduced due to the increased acid groups bonding onto the chitosan structure and reduced free volume available for feed solution molecules. Specifically, the CS-P(24) and CS-S(24) PEMs exhibited sorption values of 60.0 ± 0.3 and 59.3 ± 0.5%, respectively.

The addition of GO to the chitosan matrix resulted in a decrease water sorption to 57.4 ± 7.6% due to the inhibition of CS chain motion by the attraction from GO (Bai et al. 2015). Upon cross-linking the CS-GO membranes, water sorption was further reduced to 49.3 ± 4.7% in CS-GO-P(24) membranes and 36.7 ± 1.1% in CS-GO-S(24). While the strong ionic bonding with sulfuric acid afforded a tightly held membrane, water sorption below this value can potentially inhibit the ease of proton crossover.

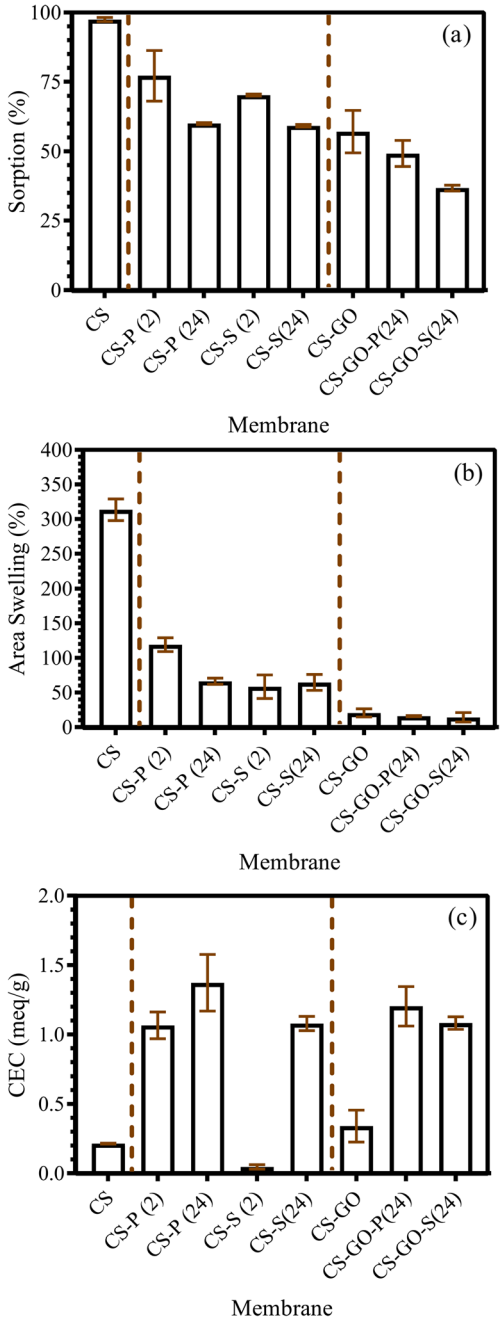

Fig. 5 Sorption (**a**), area swelling (**b**), and CEC (**c**) of the fabricated membranes

As a result of the solvent effect on polymer chains, water uptake provokes membrane swelling and subsequent chain mobility by the breakage of interchain interactions. Area swelling is therefore expected to be directly proportional to water uptake. By comparison, both the wastewater sorption and area swelling analysis (Fig. 5b) generally shared the same trend of variation; the area swelling decreased in the order of CS > CS-P(2) > CS-S(2), CS-P(2) > CS-P(24) > CS-S(24), and CS-GO > CS-GO-P(24) > CS-GO-S(24); however, despite exhibiting reduced sorption, the CS-GO-S(24)

membrane exhibited area swelling in the range similar to CS-GO-P(24) membranes. It is possible that the density of the network chain increases so much with the incorporation of GO in the CS-GO-S(24) membrane, that the sorption of wastewater molecules is reduced as well as the ability of the macromolecular chains to relax after removal from feed solution (Bajpai and Giri 2003).

Cation exchange capacity

The ratio of the content of acid groups to membrane weight responsible for the conduction of proton ions was determined by the CEC analysis, and values are presented in Fig. 5c. The presence of hydroxyl and carboxyl groups at the edge of GO, which can easily release H^+ ions in aqueous medium, contributes to the enhanced CEC of CS-GO membranes. This general trend suggests that the presence of charged acid groups in the cross-linked CS and CS-GO membranes caused an increase in CEC compared to the pristine CS and CS-GO membranes; this is due to the enhanced sorption and swelling behaviors inducing improved proton release abilities. Moreover, CEC increased with cross-linking time due to the increased number of ionic clusters and proton hopping or diffusion sites that are formed by the CS and CS-GO exposure to the SO_4^{2-} or PO_4^{3-} acid groups (Pandey and Shahi 2015; Shaari and Kamarudin 2015); these results are consistent with the observed increase in the degree of substitution with cross-linking time. The protons produced at the anode chamber are therefore allowed to hop from one proton carrier site ($–NH_2$, $–NH_3^+$, $–SO_4^{2-}$, or $–PO_4^{3-}$) which can form a hydrogen bond upon dissociating H^+ to another across the membrane, or diffuse through the MFC feed solution due to the existing electrochemical difference, where protons can combine with water molecules to produce hydronium ions (Deluca and Elabd 2006). As both proposed mechanisms depend on the membrane hydration level, these CEC results confirm the expected trends based on those observed throughout the sorption analysis and give a reliable approximation of the proton conductivity abilities of the membranes (Seo et al. 2009). For instance, the CEC increased in the order of CS < CS-GO < CS-GO-S(24) < CS-GO-P(24).

Oxygen mass transfer

The oxygen mass transfer study shows the resistance of the fabricated PEM to oxygen crossover from cathode to anode, which can affect the anaerobic atmosphere of anodic chamber. Since maintaining anaerobic condition in the anode chamber is imperative for the effective proton and electron generation due to bacterial metabolic activities, the oxygen mass transfer coefficient is an important parameter in hybrid membrane fabrication for MFC applications. In this study, the addition of GO into the CS polymeric matrix positively influenced the oxygen barrier property of the composite membranes such that CS exhibited K_o and D_o values of 4.22×10^{-3} cm/s and 3.70×10^{-5} cm^2/s, respectively, while 3.95×10^{-4} cm/s and 3.46×10^{-6} cm^2/s, respectively, were calculated for CS-GO. It was observed that greater oxygen crossover occurred through the pristine CS polymer matrix than through the mixed-matrix CS-GO membranes; this reduced oxygen permeability may be attributed to the blockage of oxygen in parts of the free volumes in the CS matrix due to the presence of GO. The CS-GO-P(24) membrane exhibited $K_o = 3.63 \times 10^{-4}$ cm/s and $D_o = 3.18 \times 10^{-6}$ cm^2/s, coherent with its higher DS, while CS-GO-S(24) membrane exhibited $K_o = 3.82 \times 10^{-4}$ cm/s and $D_o = 3.34 \times 10^{-6}$ cm^2/s. Lesser oxygen mass transfer coefficient behavior in PEM is expected to improve the performance of MFC in terms of power density generation and COD removal efficiencies by maintaining strict anaerobic conditions in the anode chamber (Venkatesan and Dharmalingam 2013).

MFC performance

Efficacy of cross-linked CS-GO mixed-matrix membranes for bioelectricity production

All membranes were studied for bioelectricity production in MFC; however, considering that CEC indicates the density of ionizable groups, which to some degree depends on trends in water sorption and area swelling and largely governs the Grothuss-type cation/proton transport mechanism across proton exchange membranes (Bai et al. 2015; Smitha et al. 2004), the CS-GO-P(24) and CS-GO-S(24) membranes were favorable membranes for MFC bioelectricity performance among all. As such, discussions herein are focused on the aforementioned mixed-matrix PEMs.

Both MFCs were operated over three fed-batch cycles, and the power generated per cubic meter of reactor volume is presented in Fig. 6. MFCs operated with CS-GO-P(24) and CS-GO-S(24) membranes similarly produced stable power

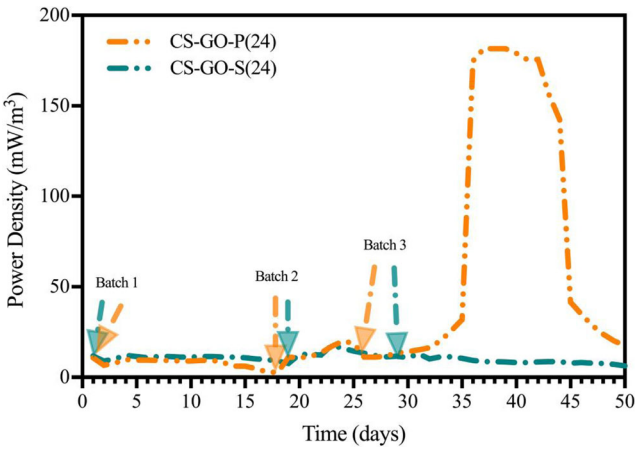

Fig. 6 Power generation over time for microbial fuel cells operated with the CS-GO-P(24) and CS-GO-S(24) membranes under 1000 Ω resistance

densities by the first batch cycle and throughout the second, indicating that the bacteria had acclimatized successfully. Continuing onto the third batch cycle, trends in power density over time began to show distinctive differences, and the MFC outfitted with the CS-GO-P(24) membrane was able to generate maximum voltage and power density of 420 mV and 181.56 mW/m^3 (day 37) compared to a maximums of 89 mV and 13.00 mW/m^3 (day 31) generated with the CS-GO-S(24) membrane. These results suggest that differences in the MFC performances over time were therefore based largely on the differences in physicochemical (for example, sorption and CEC) properties of the PEMs being used, as discussed extensively throughout the membrane characterization sections, and not limited to factors such as bacterial acclimatization.

The third batch cycle was accordingly defined as the performance cycle whereby the MFCs were operated until day 50 and underwent polarization studies as shown in Fig. 7. By day 50 of operation in an MFC and coherent with the membrane characterization trends discussed, the maximum current density and power density increased in the order of CS-GO-S(24) < CS-GO-P(24) due to the enhanced sorption properties and higher CEC afforded by the incorporation of PO_4^{3-} groups in the CS-GO matrix. Particularly, the maximum power densities of the MFCS operated with CS-GO-P(24) and CS-GO-S(24) membranes at the end of the third batch cycle were 16.35 and 6.94 mW/m^3 at current densities of 192.35 and 76.31 mA/m^3, respectively. This difference in the time-dependent behavior of the MFCs proves that cross-linking with phosphoric acid groups functions well not only for improving the thermal stability, CEC, and mechanical strength of the CS membranes but also for rendering enhanced bioelectricity, when compared to sulfuric acid cross-linking. While sulfuric acid is the stronger acid of the two, bioelectricity performance of the CS-GO-S(24) membrane may be limited by its lower physicochemical properties due to the tightly formed ionic bonds. This result is

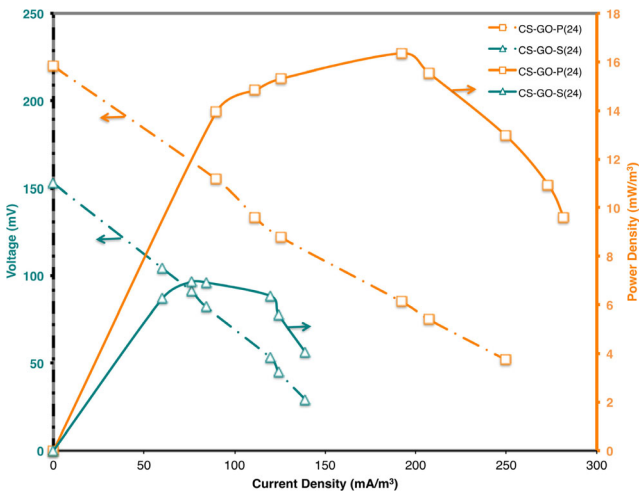

Fig. 7 Polarization curves of MFCs with cross-linked CS-GO membranes (after 50-day operation)

coherent with the internal resistances of 982 and 2650 Ω recorded for MFCs operated with CS-GO-P(24) and CS-GO-S(24) membranes, respectively, at the end of the third fed-batch cycle.

For further insight on trends in bioelectricity production for the pristine cross-linked CS membranes, these PEMs were operated over one batch cycle in the MFC, and results are shown in Table 3. Similar to the trend observed with the cross-linked CS-GO mixed-matrix composites, higher voltages and power densities were observed in MFCs operated with the phosphorylated CS PEMs than those operated with sulfurized CS PEMs. Furthermore, bioelectricity production increased with the degree of substitution of the acid group onto the amine functional group (cross-linking time).

A recent study conducted by Shahgaldi et al. (2014) demonstrated that a single culture dual-chambered MFC (200 mL working volume; 0.0012 m^2 anode electrode surface area) operated with polyvinylidene fluoride (PVDF)/Nafion (0.2 g) composite membrane produced a maximum power density of 2.9 mW/m^2 (based on anode surface area). Larger additions (0.4 g) of expensive synthetic material Nafion had to be added in order to achieve the overall maximum power density of 4.9 mW/m^2 observed throughout the study. Normalizing the power generated with the CS-GO-P(24) composite synthesized in our study to anode electrode area (0.0019 m^2), a maximum power density of 3.87 mW/m^2 was generated thereby demonstrating the potential of using low-cost and eco-friendly CS biopolymer as PEMs in MFC technology upon cheap yet efficient modification.

MFC efficiency for wastewater treatment: anolyte solution analysis

Changes in the physicochemical properties of the influent and effluent anolyte of MFCs operated with CS-GO-P(24) and CS-GO-S(24) PEMs are presented in Fig. 8. Physicochemical characteristics of the wastewater were analyzed for the MFCs operated with these membranes, as organic matter and other components present in the anolyte contribute to the metabolic

Table 3 Bioelectricity production of MFCs operated with pristine cross-linked CS membranes over one batch cycle

Membrane	Maximum voltage (mV)	Maximum power density (mW/m^3)	Current density (mA/m^3) at maximum power density
CS-P(2)	58	1.89	65.22
CS-P(24)	147	11.73	162.93
CS-S(2)	41	0.90	44.89
CS-S(24)	87	8.70	140.30

Maximum voltages were recorded throughout the batch cycle, and power and current densities were obtained in polarization studies after stepwise alteration of the resistance at the end of the cycle

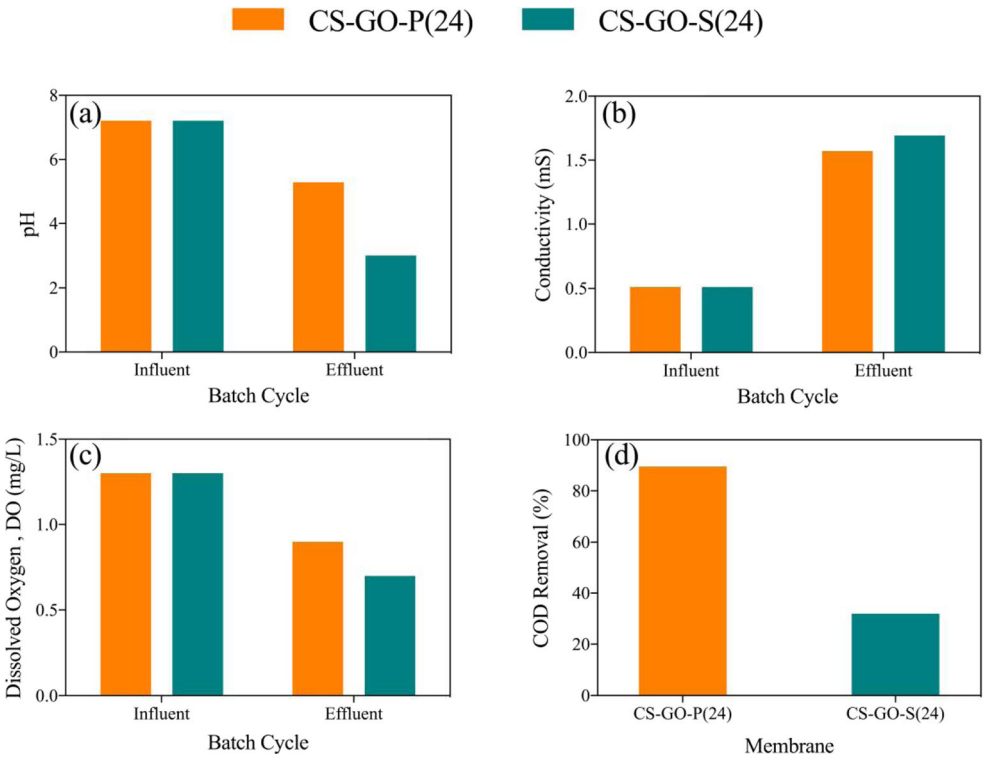

Fig. 8 Performance of MFCs (at the end of cycle 1) with CS-GO-P(24) and CS-GO-S(24) membranes as it relates to changes in **a** anolyte pH, **b** conductivity, **c** dissolved oxygen content, and **d** COD removal efficiencies

reactions that are required for the current generation and simultaneous wastewater treatment.

Anodic pH (Fig. 8a) gives an idea of the production of protons in the anode chamber due to the breakdown of organic matter by microorganisms in the wastewater and their transport from anode to cathode chamber. In both MFC systems, the influent pH was maintained as that obtained from the primary clarifier of the municipal wastewater treatment plant (pH 7.21); this close-to-neutral pH is optimal for bacterial growth in MFCs (Rozendal et al. 2008). At the end of day 18 for the CS-GO-P(24) PEM and day 19 for the CS-GO-S(24), the effluent pH of both systems had reduced to 5.29 and 3.01, respectively. Due to the H^+ production at the anode and equimolar consumption of H^+, e^-, and O_2 at the cathode, a pH decrease at the anode chamber is expected (He et al. 2008; Mohan et al. 2014; Rozendal et al. 2008). This resulting pH gradient, however, causes some potential losses and may affect the lower power output in the MFC system observed in the power density curves. While H^+ ions were being quickly replenished in the MFC systems, their transport also may not have been rapid enough for the equimolar consumption occurring at the cathode to help regulate the anodic pH near neutral. This may be attributed to the high GO content of the CS membranes which can slow proton transport.

Similar to the trend of increased H^+ production in the anode chamber, solution conductivity of both MFC systems (Fig. 8b) increased from 0.510 mS in both influents to 1.571 and 1.692 mS in the effluents of CS-GO-P(24) and CS-GO-S(24) membrane-operated MFC systems, respectively. This suggests that in the series of metabolic processes that resulted in organic matter decomposition by the bacteria in solution, ions were similarly present in both solutions for transport.

The DO concentration is an important parameter in bioelectricity generation, and results are presented in Fig. 8c. Apart from preventing substrate crossover from anode to cathode chamber, another physical function of the PEM is to restrict oxygen diffusion from the cathode to anode chamber, thereby maintaining the anoxic conditions optimum for bacterial growth in the anodic chamber necessary for H^+ and e^- generation and preventing the neutralization of H^+ released during substrate metabolism before reaching the cathode chamber (Mohan et al. 2008; Mohan et al. 2009). At the start of the MFC operation, L-cysteine was added to the anode chamber to scavenge the dissolved oxygen initially present in solution. By the end of the fed-batch cycle, DO concentration of the effluents had decreased to 0.9 and 0.7 mg/L in the MFCs operated with the CS-GO-P(24) and CS-GO-S(24) PEMs, respectively, when compared to the influent DO concentration of 1.30 mg/L for both MFCs. This result suggests that both PEMs were successful in maintaining the optimum conditions necessary for bacterial growth and current generation in the system.

As COD removal is achieved through the breakdown of organic matter by anaerobic bacteria, COD measurements allow for the investigation of MFCs as it relates to municipal wastewater treatment efficiency and the amount of organic matter successfully converted to bioelectricity. The COD removal efficiency trends shown in Fig. 8d are defined as the

ratio between the influent and effluent. COD removal efficiencies confirm that the CS-GO-P(24) membrane offered the best performance in MFC studies compared to the CS-GO-S(24); the former showed 89.52% COD removal, while the CS-GO-S(24) showed 31.99% COD removal. While many factors such as substrate and bacteria used can affect COD removal, the only difference with the MFC systems used in this study was the PEM. The differences in COD removal efficiencies observed may be due to the differences in CEC for ensuring that a continuous cycle of proton production and consumption, along with electron production and consumption, was occurring in the MFC systems.

Cumulatively, trends observed in the anolyte influent and effluent suggest that MFCs are viable for use, even at the primary clarifier stage of the wastewater treatment process, for some bioelectricity production and COD removal without a large amount of sludge production (Zhang et al. 2013). Furthermore, despite being inoculated with the same wastewater, the trend of higher COD removal efficiencies of the primary clarifier wastewater in the CS-GO-P-(24) membrane-operated MFC was coherent with its higher bioelectricity production when compared to the MFC operated with the CS-GO-S(24) PEM providing a compelling argument for the benefits of incorporating phosphoric acid groups into the structure of polymer materials.

Conclusions

Green CS-GO mixed-matrix composite membranes were fabricated and successfully cross-linked ionically by phosphorylation or sulfurization. Compared to sulfuric acid cross-linking commonly used throughout membrane studies, results have shown that phosphorylation augments further physicochemical, thermal, and mechanical stability of pristine CS and CS-GO mixed-matrix membranes. The incorporation of PO_4^{3-} groups proved superior for rendering enhanced membrane sorption behavior, which largely governs the cation exchange and proton transport processes necessary in PEMFC technology. Moreover, this study has demonstrated the potential of phosphorylated CS mixed-matrix composite membranes for use as a PEM in MFC technology to generate electricity from primary clarifier municipal wastewater. The MFC system operated with the phosphorylated CS-GO (CS-GO-P(24)) membrane generated a maximum power density of 16.35 mW/m^3 by the third fed-batch cycle compared with 6.94 mW/m^3 generated with the sulfurized CS-GO (CS-GO-S(24)) membrane. The COD removal efficiency of the CS-GO-S(24) MFC system was 31.99%, while a 2.8-fold increase in COD removal (89.52%) was achieved in the CS-GO-P(24) MFC system, providing stronger evidence for its efficiency toward enhancing the simultaneous and dual-functional wastewater treatment and bioelectricity production process. Results of this study provide some insight into the effect of the acid group incorporated into the membrane matrix and are therefore applicable to membrane enhancement studies throughout all PEMFC studies, and not limited to the enhancement of CS-based membranes.

References

Ahn MK, Lee SB, Min CM, Yu YG, Jang J, Gim MY, Lee JS (2017) Enhanced proton conductivity at low humidity of proton exchange membranes with triazole moieties in the side chains. J Membrane Sci 523:480–486. doi:10.1016/j.memsci.2016.10.018

APHA (2005) Standard methods for the examination of water and wastewater, 21st edn. American Public Health Association, New York

Azarniya A, Eslahi N, Mahmoudi N, Simchi A (2016) Effect of graphene oxide nanosheets on the physico-mechanical properties of chitosan/bacterial cellulose nanofibrous composites. Compos Part A-Appl S 85:113–122. doi:10.1016/j.compositesa.2016.03.011

Bai H, Zhang H, He Y, Liu J, Zhang B, Wang J (2014) Enhanced proton conduction of chitosan membrane enabled by halloysite nanotubes bearing sulfonate polyelectrolyte brushes. J Membrane Sci 454:220–232. doi:10.1016/j.memsci.2013.12.005

Bai H, Li Y, Zhang H, Chen H, Wu W, Wang J, Liu J (2015) Anhydrous proton exchange membranes comprising of chitosan and phosphorylated graphene oxide for elevated temperature fuel cells. J Membrane Sci 495:48–60. doi:10.1016/j.memsci.2015.08.012

Bajpai AK, Giri A (2003) Water sorption behaviour of highly swelling (carboxy methylcellulose-g-polyacrylamide) hydrogels and release of potassium nitrate as agrochemical. Carbohyd Polym 53:271–279. doi:10.1016/S0144-8617(03)00071-7

Bakangura E, Wu L, Ge L, Yang Z, Xu T (2016) Mixed matrix proton exchange membranes for fuel cells: state of the art and perspectives. Prog Polym Sci 57:103–152. doi:10.1016/j.progpolymsci.2015.11.004

Beppu MM, Vieira RS, Aimoli CG, Santana CC (2007) Crosslinking of chitosan membranes using glutaraldehyde: effect on ion permeability and water absorption. J Membrane Sci 301:126–130. doi:10.1016/j.memsci.2007.06.015

Brugnerotto J, Lizardi J, Goycoolea FM, Argüelles-Monal W, Desbrieres J, Rinaudo M (2001) An infrared investigation in relation with chitin and chitosan characterization. Polymer 42:3569–3580. doi:10.1016/S0032-3861(00)00713-8

Cadogan EI, Lee CH, Popuri SR (2015) Facile synthesis of chitosan derivatives and Arthrobacter sp. biomass for the removal of europium (III) ions from aqueous solution through biosorption. Int Biodeter Biodegr 102:286–297. doi:10.1016/j.ibiod.2015.01.018

Chen P, Hao L, Wu W, Li Y, Wang J (2016) Polymer-inorganic hybrid proton conductive membranes: effect of the interfacial transfer pathways. Electrochim Acta 212:426–439. doi:10.1016/j.electacta.2016.07.001

Czechowska-Biskup R, Jarosińska D, Rokita B, Ulański P, Rosiak JM (2012) Determination of degree of deacetylation of chitosan-comparision of methods. Progress on Chemistry and Application of Chitin and its Derivatives 17:5–20

Deluca NW, Elabd YA (2006) Polymer electrolyte membranes for the direct methanol fuel cell: a review. J Polym Sci Pol Phys 44:2201–2225. doi:10.1002/polb.20861

de Moraes ACM, Andrade PF, de Faria AF, Simões MB, Salomão FCCS, Barros EB, do Carmo Gonçalves M, Alves OL (2015) Fabrication of transparent and ultraviolet shielding composite films based on

graphene oxide and cellulose acetate. Carbohyd Polym 123:217–227. doi:10.1016/j.carbpol.2015.01.034

de Moura CM, de Moura JM, Soares NM, de Almeida Pinto LA (2011) Evaluation of molar weight and deacetylation degree of chitosan during chitin deacetylation reaction: used to produce biofilm. Chem Eng Process: Process Intensification 50:351–355. doi:10.1016/j.cep.2011.03.003

Dupuis AC (2011) Proton exchange membranes for fuel cells operated at medium temperatures: materials and experimental techniques. Prog Mater Sci 56:289–327. doi:10.1016/j.pmatsci.2010.11.001

Feng F, Liu Y, Zhao B, Hu K (2012) Characterization of half N-acetylated chitosan powders and films. Procedia Engineering 27:718–732. doi:10.1016/j.proeng.2011.12.511

Fornero JJ, Rosenbaum M, Angenent LT (2010) Electric power generation from municipal, food, and animal wastewaters using microbial fuel cells. Electroanalysis 22:832–843. doi:10.1002/elan.200980011

Fu F, Xu H, Dong Y, He M, Luo T, Zhang Y, Hao X, Ma T, Zhu C (2015) Polyphosphazene-based copolymers containing pendant alkylsulfonic acid groups as proton exchange membranes. Solid State Ionics 278:58–64. doi:10.1016/j.ssi.2015.05.018

Hajji S, Chaker A, Jridi M, Maalej H, Jellouli K, Boufi S, Nasri M (2016) Structural analysis, and antioxidant and antibacterial properties of chitosan-poly (vinyl alcohol) biodegradable films. Environ Sci Pollut R 23:15310–15320. doi:10.1007/s11356-016-6699-9

Han D, Yan L, Chen W, Li W, Bangal PR (2011) Cellulose/graphite oxide composite films with improved mechanical properties over a wide range of temperature. Carbohyd Polym 83:966–972. doi:10.1016/j.carbpol.2010.09.006

He Z, Huang Y, Manohar AK, Mansfeld F (2008) Effect of electrolyte pH on the rate of the anodic and cathodic reactions in an air-cathode microbial fuel cell. Bioelectrochemistry 74:78–82. doi:10.1016/j.bioelechem.2008.07.007

Higa M, Feng S, Endo N, Kakihana Y (2015) Characteristics and direct methanol fuel cell performance of polymer electrolyte membranes prepared from poly (vinyl alcohol-b-styrene sulfonic acid). Electrochim Acta 153:83–89. doi:10.1016/j.electacta.2014.11.155

Holder SL, Lee CH, Popuri SR, Zhuang MX (2016) Enhanced surface functionality and microbial fuel cell performance of chitosan membranes through phosphorylation. Carbohyd polym 149:251–262. doi:10.1016/j.carbpol.2016.04.118

Hummers WS Jr, Offeman RE (1958) Preparation of graphitic oxide. J Am Chem Soc 80:1339–1339. doi:10.1021/ja01539a017

Ilbeygi H, Ghasemi M, Emadzadeh D, Ismail AF, Zaidi SMJ, Aljlil SA, Jaafar J, Martin D, Keshani S (2015) Power generation and wastewater treatment using a novel SPEEK nanocomposite membrane in a dual chamber microbial fuel cell. Int J Hydrogen Energ 40:477–487. doi:10.1016/j.ijhydene.2014.10.026

Jayakumar R, Prabaharan M, Reis RL, Mano J (2005) Graft copolymerized chitosan—present status and applications. Carbohyd polym 62:142–158. doi:10.1016/j.carbpol.2005.07.017

Jiang D, Curtis M, Troop E, Scheible K, McGrath J, Hu B, Suib S, Raymond D, Li B (2011) A pilot-scale study on utilizing multi-anode/cathode microbial fuel cells (MAC MFCs) to enhance the power production in wastewater treatment. Int J Hydrogen Energ 36:876–884. doi:10.1016/j.ijhydene.2010.08.074

Justin R, Chen B (2014) Body temperature reduction of graphene oxide through chitosan functionalisation and its application in drug delivery. Mat Sci Eng C-Bio S 34:50–53. doi:10.1016/j.msec.2013.10.010

Kim DS, Guiver MD, Nam SY, Yun TI, Seo MY, Kim SJ, Hwang HS, Rhim JW (2006) Preparation of ion exchange membranes for fuel cell based on crosslinked poly (vinyl alcohol) with poly (styrene sulfonic acid-co-maleic acid). J Membrane Sci 281:156–162. doi:10.1016/j.memsci.2006.03.025

Kim JR, Cheng S, Oh SE, Logan BE (2007) Power generation using different cation, anion, and ultrafiltration membranes in microbial fuel cells. Environ Sci Technol 41:1004–1009. doi:10.1021/es062202m

Krishnamoorthy K, Veerapandian M, Zhang LH, Yun K, Kim SJ (2012) Antibacterial efficiency of graphene nanosheets against pathogenic bacteria via lipid peroxidation. J Phys Chem C 116:17280–17287. doi:10.1021/jp3047054

Liang Y, Gong C, Qi Z, Li H, Wu Z, Zhang Y, Zhang S, Li Y (2015) Intermolecular ionic cross-linked sulfonated poly (ether ether ketone) membranes containing diazafluorene for direct methanol fuel cell applications. J Power Sources 284:86–94. doi:10.1016/j.jpowsour.2015.02.159

Liu H, Logan BE (2004) Electricity generation using an air-cathode single chamber microbial fuel cell in the presence and absence of a proton exchange membrane. Environ Sci Technol 38:4040–4046. doi:10.1021/es0499344

Liu CG, Desai KGH, Chen XG, Park HJ (2005) Preparation and characterization of nanoparticles containing trypsin based on hydrophobically modified chitosan. J Agr Food Chem 53:1728–1733. doi:10.1021/jf040304v

Liu M, Zhou Y, Zhang Y, Yu C, Cao S (2013) Preparation and structural analysis of chitosan films with and without sorbitol. Food Hydrocolloid 33:186–191. doi:10.1016/j.foodhyd.2013.03.003

Liu L, Chen W, Li Y (2016) An overview of the proton conductivity of nafion membranes through a statistical analysis. J Membrane Sci 504:1–9. doi:10.1016/j.memsci.2015.12.065

Logan BE, Hamelers B, Rozendal R, Schröder U, Keller J, Freguia S, Aelterman P, Verstraete W, Rabaey K (2006) Microbial fuel cells: methodology and technology. Environ Sci Technol 40:5181–5192. doi:10.1021/es0605016

Ma J, Sahai Y (2013) Chitosan biopolymer for fuel cell applications. Carbohyd Polym 92:955–975. doi:10.1016/j.carbpol.2012.10.015

Mazaheri M, Akhavan O, Simchi A (2014) Flexible bactericidal graphene oxide–chitosan layers for stem cell proliferation. Appl Surf Sci 301:456–462. doi:10.1016/j.apsusc.2014.02.099

Min B, Kim J, Oh S, Regan JM, Logan BE (2005) Electricity generation from swine wastewater using microbial fuel cells. Water Res 39:4961–4968. doi:10.1016/j.watres.2005.09.039

Mohan SV, Mohanakrishna G, Sarma PN (2008) Effect of anodic metabolic function on bioelectricity generation and substrate degradation in single chambered microbial fuel cell. Environ Sci Technol 42:8088–8094. doi:10.1021/es8012529

Mohan SV, Srikanth S, Raghuvulu SV, Mohanakrishna G, Kumar AK, Sarma PN (2009) Evaluation of the potential of various aquatic ecosystems in harnessing bioelectricity through benthic fuel cell: effect of electrode assembly and water characteristics. Bioresour Technol 100:2240–2246. doi:10.1016/j.biortech.2008.10.020

Mohan SV, Velvizhi G, Modestra JA, Srikanth S (2014) Microbial fuel cell: critical factors regulating bio-catalyzed electrochemical process and recent advancements. Renew Sust Energ Rev 40:779–797. doi:10.1016/j.rser.2014.07.109

Oh S, Min B, Logan BE (2004) Cathode performance as a factor in electricity generation in microbial fuel cells. Environ Sci Technol 38:4900–4904. doi:10.1021/es049422p

Ordikhani F, Farani MR, Dehghani M, Tamjid E, Simchi A (2015) Physicochemical and biological properties of electrodeposited graphene oxide/chitosan films with drug-eluting capacity. Carbon 84:91–102. doi:10.1016/j.carbon.2014.11.052

Padaki M, Isloor AM, Wanichapichart P, Ismail AF (2012) Preparation and characterization of sulfonated polysulfone and N-phthloyl chitosan blend composite cation-exchange membrane for desalination. Desalination 298:42–48. doi:10.1016/j.desal.2012.04.025

Paddison SJ, Kreuer KD, Maier J (2006) About the choice of the protogenic group in polymer electrolyte membranes: ab initio modelling of sulfonic acid, phosphonic acid, and imidazole functionalized alkanes. Phys Chem Chem Phys 8:4530–4542. doi:10.1039/B611221H

Pan Y, Wu T, Bao H, Li L (2011) Green fabrication of chitosan films reinforced with parallel aligned graphene oxide. Carbohyd polym 83:1908–1915. doi:10.1016/j.carbpol.2010.10.054

Pandey RP, Shahi VK (2015) Phosphonic acid grafted poly (ethyleneimine)-silica composite polymer electrolyte membranes by epoxide ring opening: improved conductivity and water retention at high temperature. Int J Hydrogen Energ 40:14235–14245. doi:10.1016/j.ijhydene.2015.08.074

Paulchamy B, Arthi G, Lignesh BD (2015) A simple approach to stepwise synthesis of graphene oxide nanomaterial. Journal of Nanomedicine & Nanotechnology 6:1–4. doi:10.4172/2157-7439.1000253

Peighambardoust SJ, Rowshanzamir S, Amjadi M (2010) Review of the proton exchange membranes for fuel cell applications. Int J Hydrogen Energ 35:9349–9384. doi:10.1016/j.ijhydene.2010.05.017

Rao PS, Sridhar S, Wey MY, Krishnaiah A (2007) Pervaporative separation of ethylene glycol/water mixtures by using cross-linked chitosan membranes. Ind Eng Chem Res 46:2155–2163. doi:10.1021/ie061268n

Rozendal RA, Hamelers HV, Rabaey K, Keller J, Buisman CJ (2008) Towards practical implementation of bioelectrochemical wastewater treatment. Trends Biotechnol 26:450–459. doi:10.1016/j.tibtech.2008.04.008

Rudra R, Kumar V, Kundu PP (2015) Acid catalysed cross-linking of poly vinyl alcohol (PVA) by glutaraldehyde: effect of crosslink density on the characteristics of PVA membranes used in single chambered microbial fuel cells. RSC Adv 5:83436–83447. doi:10.1039/C5RA16068E

Sasikala S, Gopi KH, Bhat SD (2016) Sulfosuccinic acid-sulfonated polyether ether ketone/organo functionalized microporous zeolite-13X membrane electrolyte for direct methanol fuel cells. Micropor Mesopor Mat 236:38–47. doi:10.1016/j.micromeso.2016.08.029

Sen U, Acar O, Celik SU, Bozkurt A, Ata A, Tokumasu T, Miyamoto A (2013) Proton-conducting blend membranes of Nafion/poly (vinylphosphonic acid) for proton exchange membrane fuel cells. J Polym Res 20:1–7. doi:10.1007/s10965-013-0217-2

Seo JA, Koh JH, Roh DK, Kim JH (2009) Preparation and characterization of crosslinked proton conducting membranes based on chitosan and PSSA-MA copolymer. Solid State Ionics 180:998–1002. doi:10.1016/j.ssi.2009.04.003

Shaari N, Kamarudin SK (2015) Chitosan and alginate types of biomembrane in fuel cell application: an overview. J Power Sources 289:71–80. doi:10.1016/j.jpowsour.2015.04.027

Shahgaldi S, Ghasemi M, Daud WRW, Yaakob Z, Sedighi M, Alam J, Ismail AF (2014) Performance enhancement of microbial fuel cell by PVDF/Nafion nanofibre composite proton exchange membrane. Fuel Process Technol 124:290–295

Shanmugam A, Kathiresan K, Nayak L (2016) Preparation, characterization and antibacterial activity of chitosan and phosphorylated chitosan from cuttlebone of *Sepia kobiensis* (Hoyle, 1885). Biotechnology Reports 9:25–30

Shirdast A, Sharif A, Abdollahi M (2016) Effect of the incorporation of sulfonated chitosan/sulfonated graphene oxide on the proton conductivity of chitosan membranes. J Power Sources 306:541–551

Smitha B, Sridhar S, Khan AA (2004) Polyelectrolyte complexes of chitosan and poly (acrylic acid) as proton exchange membranes for fuel cells. Macromolecules 37:2233–2239. doi:10.1021/ma0355913

Smitha B, Sridhar S, Khan AA (2005) Solid polymer electrolyte membranes for fuel cell applications—a review. J Membrane Sci 259:10–26. doi:10.1016/j.memsci.2005.01.035

Tachaboonyakiat W, Netswasdi N, Srakaew V, Opaprakasit M (2010) Elimination of inter-and intramolecular crosslinks of phosphorylated chitosan by sodium salt formation. Polym J 42:148–156. doi:10.1038/pj.2009.317

Thakur VK, Voicu SI (2016) Recent advances in cellulose and chitosan based membranes for water purification: a concise review. Carbohyd polym 146:148–165. doi:10.1016/j.carbpol.2016.03.030

Velasquez-Orta SB, Head IM, Curtis TP, Scott K (2011) Factors affecting current production in microbial fuel cells using different industrial wastewaters. Bioresour Technol 102:5105–5112. doi:10.1016/j.biortech.2011.01.059

Venkatesan PN, Dharmalingam S (2013) Characterization and performance study on chitosan-functionalized multi walled carbon nano tube as separator in microbial fuel cell. J Membrane Sci 435:92–98. doi:10.1016/j.memsci.2013.01.064

Xie H, Tao D, Xiang X, Ou Y, Bai X, Wang L (2015) Synthesis and properties of highly branched star-shaped sulfonated block poly(arylene ether)s as proton exchange membranes. J Membrane Sci 473:226–236. doi:10.1016/j.memsci.2014.09.015

Xiong Y, Liu QL, Zhang QG, Zhu AM (2008) Synthesis and characterization of cross-linked quaternized poly (vinyl alcohol)/chitosan composite anion exchange membranes for fuel cells. J Power Sources 183:447–453. doi:10.1016/j.jpowsour.2008.06.004

Yadav M, Ahmad S (2015) Montmorillonite/graphene oxide/chitosan composite: synthesis, characterization and properties. Int J Biol Macromol 79:923–933. doi:10.1016/j.ijbiomac.2015.05.055

Yang X, Tu Y, Li L, Shang S, Tao XM (2010) Well-dispersed chitosan/graphene oxide nanocomposites. ACS Appl Mater Interfaces 2:1707–1713. doi:10.1021/am100222m

Zhang F, Ge Z, Grimaud J, Hurst J, He Z (2013) In situ investigation of tubular microbial fuel cells deployed in an aeration tank at a municipal wastewater treatment plant. Bioresour Technol 136:316–321. doi:10.1016/j.biortech.2013.02.107

Zhao Y, Fu Y, Hu B, Lü C (2016) Quaternized graphene oxide modified ionic cross-linked sulfonated polymer electrolyte composite proton exchange membranes with enhanced properties. Solid State Ionics 294:43–53. doi:10.1016/j.ssi.2016.07.002

Zhu N, Chen X, Zhang T, Wu P, Li P, Wu J (2011) Improved performance of membrane free single-chamber air-cathode microbial fuel cells with nitric acid and ethylenediamine surface modified activated carbon fiber felt anodes. Bioresour Technol 102:422–426. doi:10.1016/j.biortech.2010.06.046